RSC Advances

ROYAL SOCIETY
OF **CHEMISTRY**

www.rsc.org/advances

Journal Name

ARTICLE

Aggregation-induced emission in fluorophores containing hydrazone structure and sulfone central: restricted molecular rotation

Jing Li[a], Wen Yang[a], WeiqunZhou[a]*, Chunchun Li [a], Zhongqing Cheng[b], Mengying Li [b], Liqun Xie [c] , Youyong Li [d]

Four 4, 4'-Di((E)-2-(4-4-alkoxyaniline)hydrazinyldiphenyl sulfones of D-π-A-π-D were synthesized and their structures were characterized by NMR, IR, and element analysis. These compounds displayed weak fluorescence emission in THF while fluorescence enhancement in THF/water mixture solvent. Fluorescent microscope imaging showed the formation of the aggressive state. The mechanism of aggregation-induced emission (AIE) was supported by molecular dynamic calculations. The intermolercular hydrogen bonds between adjacent molecules inhibited the intramolecular rotations, preventing π-π stacking and causing AIE enhancement. Living cell imaging experiments opened up a new way to cell fluorescence staining.

1. Introduction:

The main organic photoimaging materials are of great importance in photochemical and applied chemical field [1-5]. Significant developments have taken place in the past few years leading to practical organic photoimaging materials. Outstanding fluorescent materials are often designed with large conjugated systems [6-10], so the conventional structural design strategy of organic fluorophores enlarged the extent of π-conjugation by melding more and more aromatic rings together. Although the bigger conjugate structure can produce high fluorescence in the dilute solutions, the fluorescence can be usually quenched in concentrated solutions and solid state. This phenomenon is usually called aggregation-caused fluorescence quenching (ACQ) because of π-π stacking and other non-radiative pathways [11]. The ACQ effect has restricted the real-world applications of fluorescent materials [12,13]. For example, as common organic materials are insoluble in water, the materials of the ACQ effect cannot be used as sensors to detect biological molecules in physiological buffers and monitor ions in river water [14,15]. Since the luminescent materials as the light-emitting devices must be fabricated in a solid film form, the ACQ effect materials cannot be used to the fabrication of efficient organic light-emitting diodes (OLEDs) [16-24].

In 2003, Tang et al. had synthesized TTPEPy [25] with high fluorescent efficiency and high AIE effect which overcame ACQ effect. The appearance of AIE made it possible to apply the organic photoimaging materials in the real-world applications.

It is realized that rational restricted intramolecular rotation (RIR) closed the possible non-radiative decay channels and activated radiative decay channels, which led to the strong fluorescence [26,27,28]. Some typical examples of the AIE systems have been developed such as hexaphenylsilole (HPS) [29] with a propeller-shaped non-planar molecule, butterfly-shaped pyran derivatives [30], cyano-substituted biphenyl ethylene with J-aggregation typed spatial structure [31], and BODIPY dyes with V-shaped structure [32]. V-shaped compounds have the twisted nonplanar structures to prevent π-π stacking and induce the fluorescence enhancement in the aggregated states. For instance, V-shaped BODIPY [32] is able to reduce the close intermolecular interactions and correspondingly improve solid state emission of the BODIPY dyes. V-shaped pyridinium salts DMDPN [33] has also exhibited a typical aggregation-induced emission behavior.

Usually, D-π-A-π-D type fluorescent materials have become an efficient way for designing brilliant fluorescence materials for they emit stronger intramolecular charge transfer (ICT) fluorescence. For example, V-shaped D-π-A-π-D compound BCPPM exhibited strong ICT fluorescence in the solid state [34]. In this article, we synthesized four V-shaped compounds of D-π-A-π-D, 4, 4'-Di((E)-2-(4-4-alkoxyaniline)hydrazinyldiphenyl sulfone (BAHDS1-4), where the sulfone unit served as the central acceptor core, two hydrazinyldiphenyl conjugated chains served as the π-bridge to extend the conjugation

[a] School of Chemistry & Chemical Engineering and Material Science, Soochow University, 199 Ren'ai Road, Suzhou, People's Republic of China, 215123
[b] School of Biology and Basic Medical Sciences, Soochow University, 199 Ren'ai Road, Suzhou, 215123, People's Republic of China, 215123
[c] Gold Mantis school of Architecture, Soochow University, 199 Ren'ai Road, Suzhou, People's Republic of China, 215123
[d] Functional Nano & Soft Materials Laboratory, Soochow University, 199 Ren'ai Road, Suzhou, People's Republic of China, 215123

length, and methoxy, n-butoxy, tert-butoxy and 4-phenoxy was introduced as donor units. The larger substituent group such as n-butoxy, tert-butoxy and phenoxy were introduced to restrict the intramolecular rotation and enhance fluorescence emission. Four compounds emitted weak fluorescence in THF, but the fluorescence gradually enhanced with the addition of the non-soluble water in THF and presented AIE effect.

2. Experimental section

2.1 Materials and instruments

Bis(4-chlorophenyl)sulphone, hydrazine hydrate(85%), 4-methoxybenzaldehyde, 4-n-butoxy benzaldehyde, 4-t-butoxy benzaldehyde, 4-methoxybenzaldehyde, THF, DMSO, acetone, acetonitrile and DMSO-D$_6$ were purchased from J&K (CHINA). Melting points were measured on a Kofler melting point apparatus and uncorrected. IR spectra were obtained in KBr discs using a Nicolet 170SX FT-IR spectrometer. Elemental analyses were performed on a Yannaco CHNSO Corder MT-3 analyzer. ^{1}H NMR and ^{13}C NMR has been recorded respectively on INOVA 400 at 400 and 100MHz, with TMS as internal standard, DMSO-D$_6$ as deuterated solvents and chemical shifts reported as ppm. Mass spectra were recorded on a Finnigan MAT95 mass spectrometer. The absorption and fluorescence spectra were recorded on a CARY50 UV-VIS spectrophotometer and an FLS920 fluorescence spectrophotometer. The Quantum Yield (QY) of the as-synthesized BAHDS derivatives was calculated based on the following equation: $\Phi_f = \Phi_r \cdot \frac{I_{BAHDS}}{I_R} \cdot \frac{A_R}{A_{BAHDS}}$. Φ_f is the fluorescence quantum yield, I is the intensity of the fluorescent spectra, and A is the optical density at excitation wavelength. QY was measured by taking anthracene as a standard for BAHDS. R referred to the standard anthracene with known quantum yield. Film samples for the measurements of UV-vis and fluorescence spectroscopy were prepared by drop casting and the subsequent spin-coating (2000 rpm, 30 s) from THF solutions (100 mL) on quartz cell (12.5 ×12.5×45 mm). The fluorescence microscope imaging of the aggregations was obtained by Leica DM2500M. The cell images were gathered with the inverted fluorescence microscope (Olympus, IX71) and processed with Nikon AY software. The scanning electron microscope (SEM) images of the aggregations were obtained by Hitachi S4800. All the experiments were carried out at room temperature.

2.2 Cell culture and fluorescence imaging

A549 cells (human lung adenocarcinoma cell) were purchased from the Shanghai Institute of Cell Biology. The cells were cultured in Roswell Park Memorial Institute culture medium (RPMI-1640), supplemented with 6% calf serum, penicillin (100 U·mL^{-1}), streptomycin (100×10^{-6} g·mL^{-1}) and 2.5×10^{-4}mol·L^{-1} L-glutamine at 37°C in a 5% CO$_2$ incubator. The cells were cultured in a 15 mm diameter cell culture dish for 2 days. A549 cells were incubated with the aggregations at a final concentration of 50 μg·mL^{-1} for 30 min, and washed with PBS buffer to remove extra cellular material. Then the dish placed to get a long-term imaging under an inverted fluorescence microscope (Olympus, IX71) at 450 nm (λ = 380 nm).

2.3 Computational methods

The ground and excited states of molecules were optimized with the Becke-3-Lee-Yang-Parr (B3LYP) [35-37] by density functional theory (DFT) and time-dependent DFT (TD-DFT) calculations at the level of 6-311G(d) with Gaussian 09 program [38]. TD combining with a SCRF method [39] (CPCM, by THF as solvent) at the same level were applied to indicate the energies of HOMO and LUMO. The vibrational frequencies calculations were also performed to ensure the stability of the calculation result and to avoid virtual frequency.

The MD(molecular dynamic) simulations were performed by Discover module within Materials Studio 7.0 with the COMPASS force field for the studied molecular with the amorphous cell [40]. It was carried out with constant temperature and constant volume ensemble (NVT). The temperature was set at 300K and kept constant using a nose thermostat [41]. Pressure was set at 1 atm. Electrostatic energies were calculated by the vdW & Coulomb method with a 9.5-Å non-bonded cutoff. the total simulation time was 10.0ps and each step took 1.0fs.

3. Result and Discussion

3.1 Synthesis

The synthetic route was shown in Scheme 1.

3.1.1 4, 4'-Dihydraziondiphenyl sulfone

Two to three drops of triethylamine were added to a suspension of 4,4'-dichlorodiphenyl sulfone (5.74g, 0.02mol) and 50mL hydrazine hydrate(85%) in the round flask (250mL). Then the mixture was reflux for 24 hours until the solid completely dissolved. The resulting solution was cooled and diluted with ice water; the precipitate was removed by filtration, washed to neutrality with water, and dried over KOH. The yield was 5.0g (90.0%). Found: M$^+$, 278; calculation, 278.

#### 3.1.2 Bis 4,4'-((E)-2-(4-4-alkoxyaniline) hydrazinyldiphenyl sulfone(BAHDS)

The mixtures of 4-alkoxybenzaldehyde (0.0045 mol) and 4, 4'-dihydraziondiphenyl sulfone (0.002 mol) dissolved in 10 ml of dioxane. After stirred at 60°C for 2 h, the reaction mixtures were cooled to room temperature. The solvents were removed by evaporation. The obtained product was washed with water for three times, and dried over anhydrous MgSO$_4$ to yield the product. Those structures were analysed by elemental analysis, ^{1}H NMR, ^{13}C NMR and IR.

BAHDS-1: White powder. Yield: 78%. m.p.: 259.6°C. Anal. calc. formula: C$_{28}$H$_{26}$N$_4$O$_3$S. (%): C, 65.35; N, 10.89; H, 5.09. Found (%):C, 65.38; N, 10.72; H, 5.12. ^{1}H-NMR (400 MHz, DMSO-D6) δ 10.79 (s, 2H), 7.94 (s, 2H), 7.68 (dd, J=9.2Hz, 8.8Hz, 8H), 7.16 (d, J = 8.8 Hz, 4H), 7.01 (d, J = 8.8 Hz, 4H), 3.61(s, 6H). ^{13}C-NMR (100 MHz, DMSO-D6) δ 50.22(CH$_3$) 111.46(Ph) 114.23(Ph) 127.64(Ph-C) 128.73(Ph) 130.65(Ph-S) 139.86(C=N) 148.77(Ph-N) 159.89(Ph-O). FT-IR (ν, cm^{-1}): 3304 (ν$_{N-H}$) 2930, 2837 (ν$_{C-H}$) 1598 (ν$_{C=N}$)1279, 1105 (ν$_{SO2}$), 1030 (ν$_{C-O}$).

BAHDS-2: White powder; Yield: 74%. m.p.: 225.5°C. Anal. calc. formula: $C_{34}H_{38}N_4O_3S$. (%): C, 68.20; N, 9.36; H, 6.40. Found (%):C, 68.32; N, 9.41; H, 6.38. ^{1}H-NMR (400 MHz, DMSO-D6) δ 10.78 (s,2H), 7.93 (s, 2H), 7.67 (dd, J=9.2Hz, 8.8Hz, 8H), 7.15 (d, J = 8.8 Hz, 4H), 6.99 (d, J = 8.8 Hz, 4H), 4.02(t, J = 6.4Hz, 4H), 1.72(m, 4H), 1.46(m, 4H), 0.96(t, J = 7.2Hz, 6H) ^{13}C-NMR (100 MHz, DMSO-D6) δ 13.70(CH_3) 18.72(C-C) 30.71(C-C) 67.24(C-O) 111.44(Ph) 114.69(Ph) 127.52(Ph-C) 128.72(Ph) 130.62(Ph-S) 139.89(C=N) 148.77(Ph-N) 159.35(Ph-O) FTIR (ν, cm^{-1}): 3328 (v_{N-H}), 3092, 2962, 2879 (v_{C-H}), 1593 ($v_{C=N}$), 1273, 1098 (v_{SO2}), 1022 (v_{C-O})

BAHDS-3: White powder; Yield: 73%. m.p.: 195.1°C. Anal. calc.formula: $C_{34}H_{38}N_4O_3S$. (%): C, 68.20; N, 9.36; H, 6.40. Found (%):C, 68. 27; N, 9.41; H, 6.38. ^{1}H-NMR (400 MHz, DMSO-D6) δ 10.85 (s,2H), 7.95 (s, 2H), 7.67 (dd, J=9.2Hz, 8.4Hz, 8H), 7.16 (d, J = 8.8 Hz, 4H), 7.03 (d, J = 8.4 Hz, 4H), 1.35(s, 18H) ^{13}C-NMR (100 MHz, DMSO-D6) δ 28.56(CH_3) 78.47(C-C) 111.53(Ph) 123.53(Ph) 127.00(Ph-C) 128.76(Ph) 129.84(Ph) 130.79(Ph-S) 139.64(C=N) 148.70(Ph-N) 155.90(Ph-O) FTIR (ν, cm^{-1}): 3290 (v_{N-H})，3115, 2978 (v_{C-H}), 1593 ($v_{C=N}$), 1273, 1098 (v_{SO2}), 1022 (v_{C-O}).

BAHDS-4: Yellow powder; Yield: 68%. m.p.: 178.4°C. Anal. calc.formula: $C_{38}H_{30}N_4O_3S$. (%): C, 73.29; N, 9.00; H, 4.86. Found (%):C, 72.98; N, 9.11; H, 4.56. ^{1}H-NMR (400 MHz, DMSO-D6) δ 10.89 (s,2H), 7.98 (s, 2H), 7.73 (d, J= 9.2Hz, 7.2Hz, 8H), 7.45 (t, J= 8.0 Hz, 4H), 7.19 (m, 6H), 7.08 (t, J = 8.8 Hz, 8H). ^{13}C-NMR (100 MHz, DMSO-D6) δ 111.46(Ph) 118.93(Ph) 123.81(Ph) 127.91(Ph-C) 128.77(Ph) 130.33(Ph) 130.90(Ph-S) 139.86(C=N) 148.77(Ph-N) 159.89(Ph-O). FTIR (ν, cm^{-1}): 329 (δ_{N-H}) ，3067, 3042 (δ_{C-H}), 1591 ($\delta_{C=N}$), 1273, 1105 (δ_{SO2}), 1061 (δ_{C-O}).
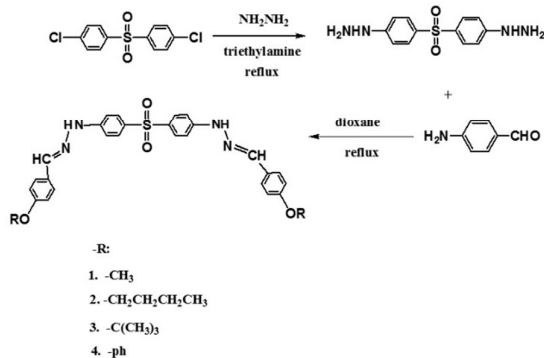
Scheme 1 The synthetic route of BAHDS
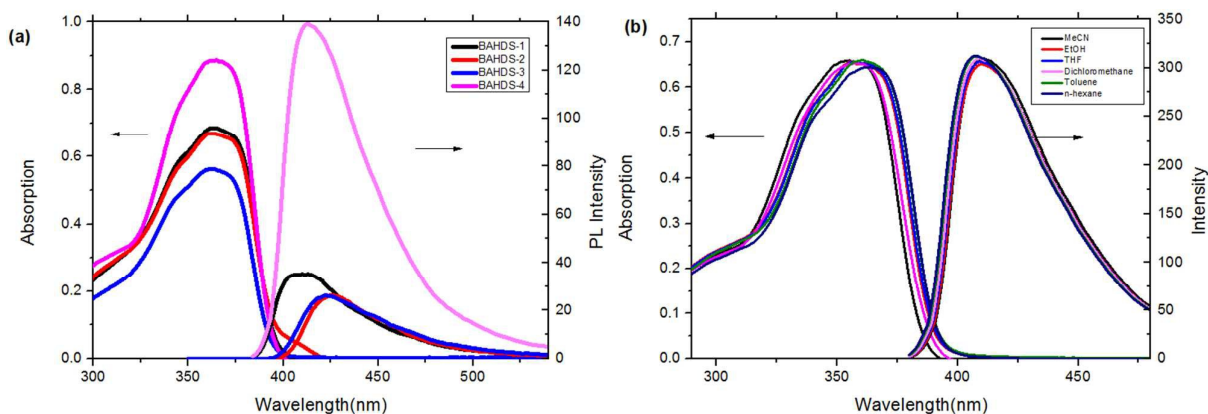
3.2 Photo-physical properties

Fig.1(a) showed UV absorption and fluorescence emission of BAHDS derivatives in THF. Four BAHDS derivatives have similar absorption and emission curves because of similar molecular structure. The maximum absorption wavelength was located at 355-365nm. The very weak fluorescent emissions were displayed under a 365nm UV lamp, and the fluorescence quantum yield was lower than 1% (Table1). The UV-vis spectra and fluorescent spectra of BAHDS-1 in different solvents were recorded in Fig.1 (b). The slightly red-shift with the polarity increase of the solvents were observed in UV spectra. Stocks shift (Δλ) was between 55 and 60 nm. Both of the moderate Stocks shift (Δλ =55~60 nm) and the characteristics of wavelength red-shift indicated the π-π* transition of the absorption.

Optimized molecular structures at B3LYP/6-311G(d) level and molecular orbital amplitude plots of HOMO and LUMO for BAHDS derivatives were depicted in Fig.2. Because of their similar structures, BAHDS 1-4 have similar HOMO, LUMO. Take BAHDS-1 as an example: the hydrazine moiety of two sides conjugated to the adjacent two benzene rings consisting of a π conjugated plane separately. Two side π conjugated planes intersected at sulfone and formed V-shaped D-π-A-π-D molecular structures (the sulfone as the central acceptor core, two hydrazinyldiphenyl conjugated chains as the π-bridge to extend the conjugation length, and methoxy, n-butoxy, tert-butoxy and 4-phenoxy as donor separately). The charges of HOMO were focused on the hydrazone moiety and its nearby phenyl ring, while charges of LUMO were centred on sulfone moiety, which indicated the intramolecular charge transition (ICT) of HOMO to LUMO.

Fig. 1(a) UV-Vis absorption and fluorescence emission of BAHDS derivatives in THF (1×10^{-5}mol·L^{-1}). (b) UV-vis and fluorescent spectra of BAHDS-1 in different solvents (1×10^{-5}mol·L^{-1})

Table 1 the maximum absorption wavelength (λ_{ab}, nm), emission wavelength, (λ_{em}, nm) and fluorescence quantum yield (Φ_f, %) of BAHDS derivatives in THF and THF/water

	THF			*THF-water*				*film*
	λ_{ab}(nm)	λ_{em}(nm)	Φ_f(%)	λ_{em}(nm)	Φ_f(%)	water(%)	I/I$_0$*	λ_{em}(nm)
BAHDS-1	365	408	0.04	433	2.7	93	66.6	432
BAHDS-2	364	423	0.03	433	6.9	93	228.4	433
BAHDS-3	365	423	0.03	423	5.7	70	190.4	423
BAHDS-4	363	413	0.16	438	22.4	90	140.0	437

*I/I$_0$:the proportion of Φ_f in THF to Φ_f in THF-water

Time-dependent density functional theory calculation (TD-DFT) were applied to indicate the energies of HOMO and LUMO. Table 2 showed the energy gaps between the HOMO and LUMO orbitals of DFT predicted and UV absorption. From Table 2, the calculated energy gaps between the HOMO and LUMO were close to the corresponding UV absorption energies with a difference value of 0.15eV, 0.18eV, 0,19eV, 0.22eV for BAHDS1-4 respectively. The distinction between the calculations and experiments was in the acceptable ranges to indicate the significance of DFT calculations.
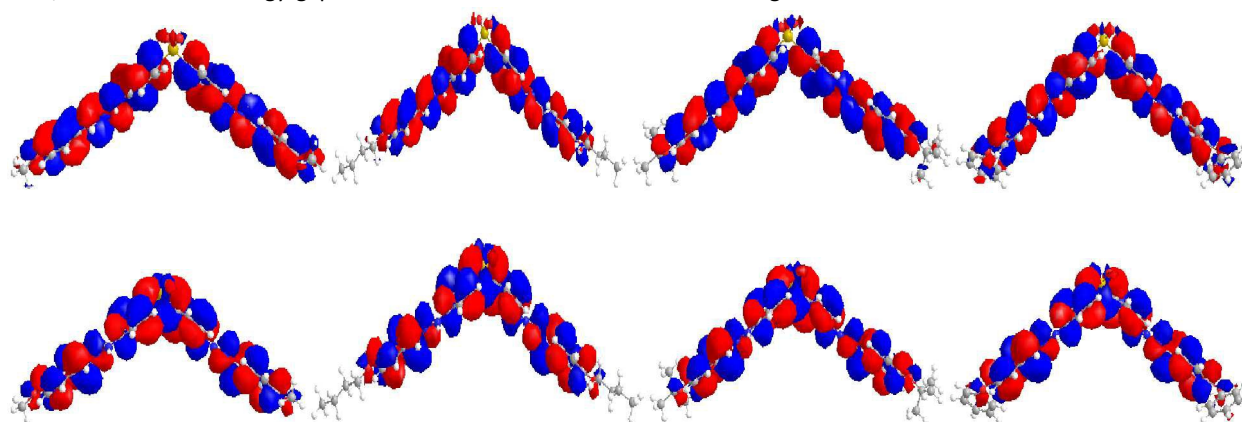

Fig.2 HOMO(top) and LUMO(bottom) orbitals of BAHDS-1 BAHDS-2 BAHDS-3 and BAHDS-4 computed by the B3LYP/6-311G(d) level of the theory from left to right.

Table 2 Energy gaps of UV and TD-DFT (B3LYP/6-311G(d)/SCRF)

	Experimental(eV)	*Calculated(eV)*	*HOMO (eV)*	*LUMO(eV)*
BAHDS-1	3.40 (365nm)	3.25	-5.40	-1.68
BAHDS-2	3.41 (364nm)	3.23	-5.40	-1.70
BAHDS-3	3.40 (365nm)	3.21	-5.36	-1.69
BAHDS-4	3.42 (363nm)	3.20	-5.48	-1.81

3.3 Aggregation-Induced Properties

A poor-solvent photoluminescence (PL) test, commonly used for studying the AIE phenomenon [42-44], was performed to explore the luminescent behaviour of the prepared BAHDS derivatives. As water was a poor solvent of BAHDS 1-4, the molecules would aggregate in THF/water mixtures with high water contents. Thus, the luminescence from such systems primarily attributed to molecule aggregation, not the solute molecules. AIE effect (I/I$_0$) of BAHDS derivatives was shown in Fig.3 and Table 1. In Fig.3, the changes of UV in THF/water mixtures with varying water volume fractions could confirm the formation of aggregate in BAHDS. BAHDS-1 exhibited an absorption peaks at 365 nm in pure THF solution (Fig

3(a)). With an increase in fw (water volume fraction) from 0% to 80%, the absorption peaks basically remained at the same positions. However, when the fw increased to 90%, the shoulder absorption peak at about 300 nm rose. Meanwhile, the leveled-off tails appeared in the visible region when fw equal to 90%, indicating that aggregates were probably at nanoscale sizes. When fw≤80%, no leveled-off spectral tails in the long-wavelength region confirmed that the molecules dissolved as isolated species in the solvent mixture. A very weak fluorescence emission was observed in pure THF with Φ_f = 0.04% (Table 1). Similar to the UV spectra, the fluorescence spectra exhibited no obvious changes as the content of water increased from 0% to 80%. A dramatic fluorescence enhancement was observed when fw equal to 90%. When fw equal to 93%, the fluorescence increased to a maximum value, the intensity was 66.6 times (Table 1) higher than that in pure THF, and the fluorescence quantum yield increased to 2.7% (Table 1). In addition, the maximum emission wavelength showed a red shift of 24 nm, which indicated that aggregates were probably at nanoscale sizes [45].
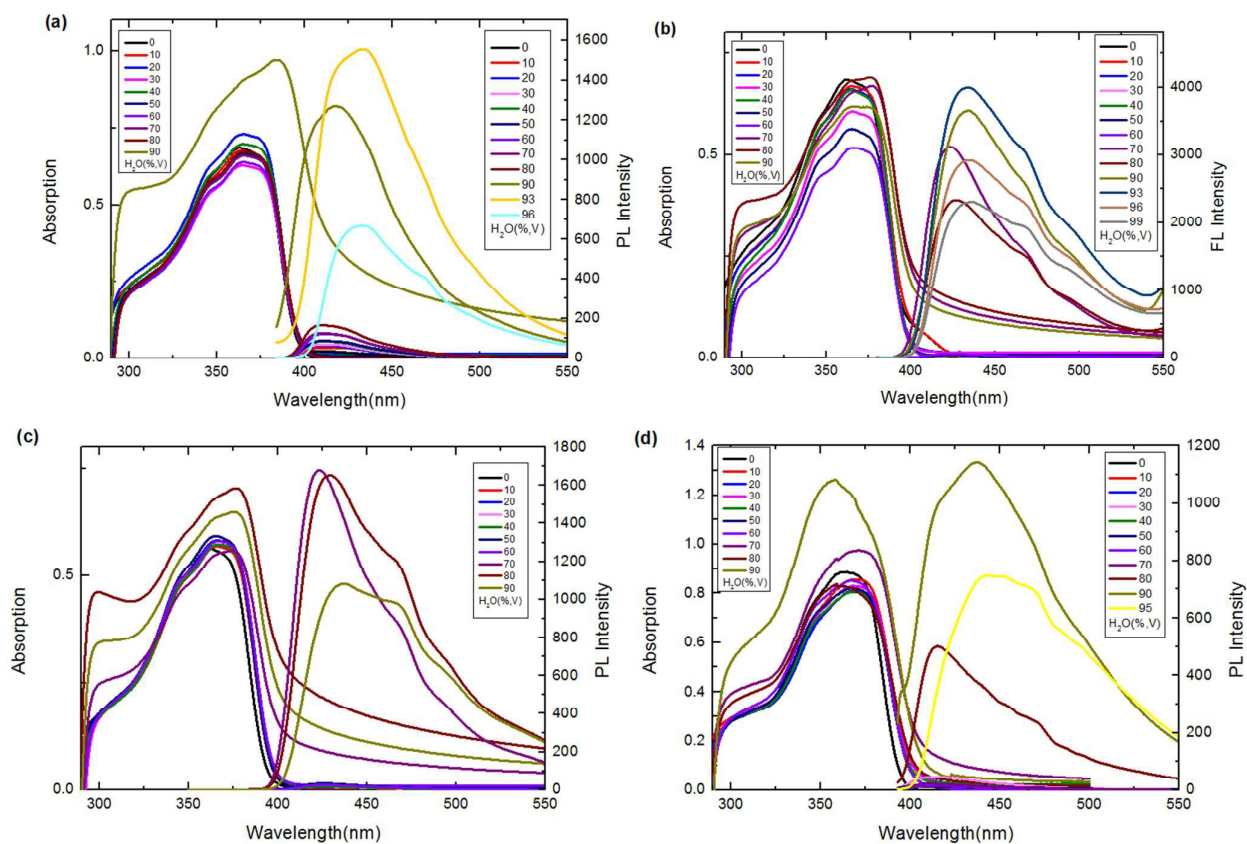
Journal Name

ARTICLE

Fig.3 UV-vis and emission spectra of BAHDS-1 (a), BAHDS-2 (b), BAHDS-3 (c) and BAHDS-4 (d) in THF-water mixtures (5×10^{-5} mol·L^{-1}),

Our strategy toward increasing the steric hindrance of substituted group was introducing the larger alkoxy, n-butoxyl, tert-butoxyl and phenoxyl into the phenyl cycle of the molecules, which could prevent π-π stacking and was beneficial to AIE effects of BAHDS derivatives. In Fig.3 (b), Fig.3(c) and Fig.3(d) as fw increased to 70%, the shoulder absorption peak appeared and the leveled-off tails appeared in the visible region, indicating the formation of aggregates states for all of BAHDS-2,3,4. It can be found that both BAHDS-2 and BAHDS-3 exhibited outstanding fluorescence enhancement for fw> 70% in the THF/water solutions. The maximum emission enhancements of 228.4-fold(fw = 93%), 190.4-fold (fw =70%) (Table 1) for BAHDS-2 and BAHDS-3 respectively are larger than that of BAHDS-1 in THF/water (66.6-fold), and their fluorescence quantum yields were measured to be 6.9% and 5.7%. Moreover, the maxima emission wavelengths shifted red 10-20nm.

As shown in MD calculations (Fig. 4), an intramolecular hydrogen bond interaction was found in BAHDS-4. It affected the vibration of BAHDS-4 and increasing of the rigidity of molecule, which benefited to the fluorescence enhancement in THF solution. As shown in

Table 1, the fluorescence quantum yield of BAHDS-4 was 0.16% in THF. The further investigated aggregation fluorescence in THF/water solutions showed BAHDS-4 exhibited the large fluorescence enhancement for fw to 80 % in Fig.3 (d). When the water fractions increased to 90 %, the intensity reached to the maximum, the emission enhanced 140 times (fw= 90%) compared with BAHDS-4 in THF(Table1), and the Φ$_f$ increased to 22.4%, the largest in BAHDS 1-4. Additionally, the emitted wavelength red shifted from 422 nm of BAHDS-1 to 438 nm of BAHDS-4.
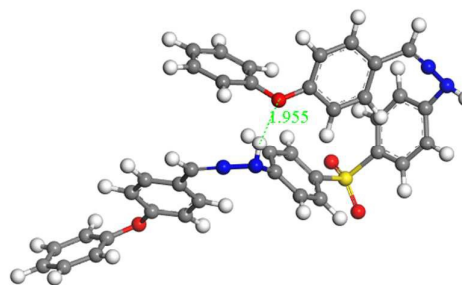

Fig.4 molecular dynamic calculation of BAHDS-4 in THF solution

RSC Advances Accepted Manuscript

As we can envisage, the steric hindrance relevant to phenyl rings was gradually enhanced with increasing substituted groups. The steric hindrance of the substituted groups, n-butoxy, tert-butoxy and phenoxy were larger than methoxyl in BAHDS system, and the motion or vibration of the phenyl rings were suppressed in aggregation states, which led to the enhanced fluorescence. In comparison with BAHDS-2 and BAHDS-3, because of the p-π conjugation between oxygen and phenyl, the rigidity of BAHDS-4 molecule probably improved as well, on account of the steric repulsion of the large groups, giving rising to fluorescence quantum yields boosting from 0.01 (BAHDS-1) to 0.16 (BAHDS -4) in THF solution (Table 1). Namely, by internal control through the introduction of alkoxylgroups, the PL properties of the BAHDS derivatives can be modulated. This indicated that steric congestion of the relevant substituted can fix the molecules and significantly inhibit the non-radiance annihilation process, leading to the high luminescence of BAHDS-4 even in dilute solution. Based on steric hindrance, by the introduction of para- alkoxylin the BAHDS unit, the triggered RIR as the fundamental mechanism of the intriguing AIE phenomenon was directly verified through simple chemical modifications. Probably, the investigations on AIE phenomenon can give us a definite understanding of the mechanism of AIE

characteristics, which will be also beneficial for the novel molecular design.

Fig. 5(a) displayed SEM image of BAHDS derivatives. In the image of SEM, the diameter of nanoscale size of BAHDS derivatives in THF/water was about 500nm. BAHDS-1 and BAHDS-4 were sphere shaped nanostructure, and BAHDS-2 and BAHDS-3 were needle like nanoscale structures .Fluorescence microscope image of BAHDS derivatives under UV irradiation was showed in Fig.5(b). The nanoscale particles of BAHDS1-4 emitted strongest bright blue fluorescence under illumination with a 365nm UV lamp. The formation of aggregation state could also be proved by the level-off tail stretching into the longer wavelength region in film state in Fig.5(c). Calculations of full-width half maximum (fwhm) revealed that the emission spectra of the BAHDS in the solid state were comparable and narrower as compared to the emission spectra obtained in THF/water. Formation of higher order aggregates in water or solution resulted in such narrower and higher intensity emission bands because of reduced intermolecular interactions. The packing efficiency and intermolecular interactions also contribute to enhanced luminescence.
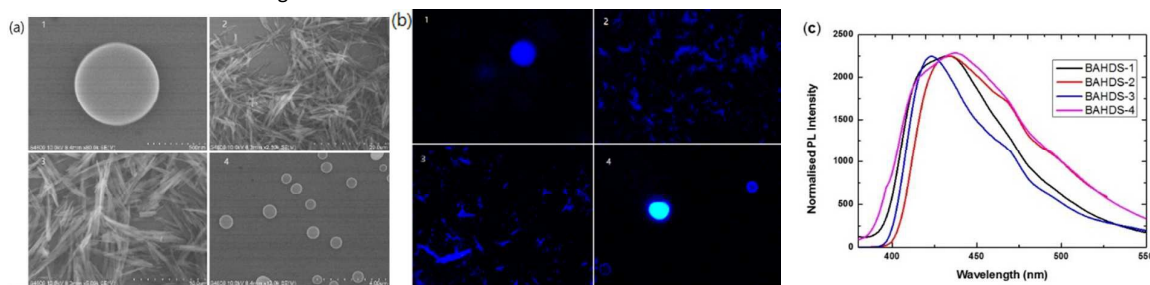

Fig. 5(a) SEM image of BAHDS-1 (1), BAHDS-2 (2), BAHDS-3 (3), BAHDS-4 (4) under UV irradiation. (b) Fluorescence microscope image of BAHDS-1 (1), BAHDS-2 (2), BAHDS-3 (3), BAHDS-4 (4). (c) Normalised PL spectra of BAHDS derivatives in film state.

Fluorescence spectral measurement was determined every six hours until forty-eight hours. It was shown in Fig. 6(a) that with the increasing standing time of BAHDS derivatives, few change could be observed. It showed that strong aggregation induced fluorescence

of BAHDS derivatives could remain stable for a long time. Also, Fig. 6(b) indicated the excellent stability of BAHDS derivatives in a large range of pH from 3 to 8.
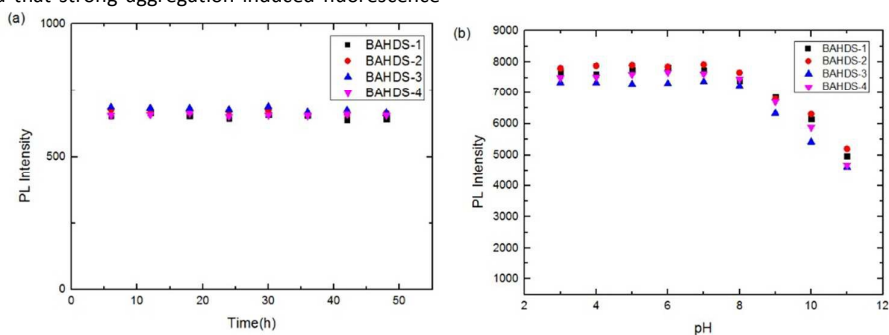

Fig.6 Normalized PL spectra of BAHDS 1-4 (10μM in THF/Water solvent) at different standing time (a) and different pH (b).

3.4 Mechanism of the AIE of BAHDS

To find the links between AIE and the packing mode in the solid state, molecular dynamic calculation of BAHDS-1, BAHDS-2 and BAHDS-4 were performed. Fig.7(a) showed the molecular dynamic

calculation of the packing of BAHDS-1. In Fig.7, the main intermolecular interactions existed in O…H, and the distance between O and H were 2.774Å and 2.467Å respectively (Fig.7(a)).

　　　ARTICLE

The intermolecular interaction forced tortuosity of the molecules, which prevented the face-to-face packing mode, and caused AIE enhancement: I/I_0 was 66.6 times (Table 1). Fig.7(b) showed the molecular dynamic calculation of BAHDS-2. Different from BAHDS-1, the intermolecular hydrogen bonds were found in BAHDS-2 (Fig. 7(b)). The distance between O and H were 1.858Å and 1.818Å. The intermolecular hydrogen bonding interaction inhibited the intramolecular rotation[46-48], which benefited to AIE enhancement. Similar to that in BAHDS-1, face-to-face stacking was not found.

Both two reasons above increased AIE effect(I/I_0 = 228.4 times (Table 1)). Because of similar structures, we did not calculate the packing mode of BAHDS-3. We held that the mechanism of AIE enhancement was similar to that of BAHDS-2 (I/I_0 = 190.4). In the packing mode of BAHDS-4, the intermolecular hydrogen bonding interaction were also found and the distance of O...H were 1.879Å, 1.955Å, 1.875Å and 1.826Å respectively. Strong hydrogen bonds in BAHDS-4 held the structure of BAHDS-4 more securely, thus the bond vibration decreased and AIE increased (I/I_0 = 140.0).
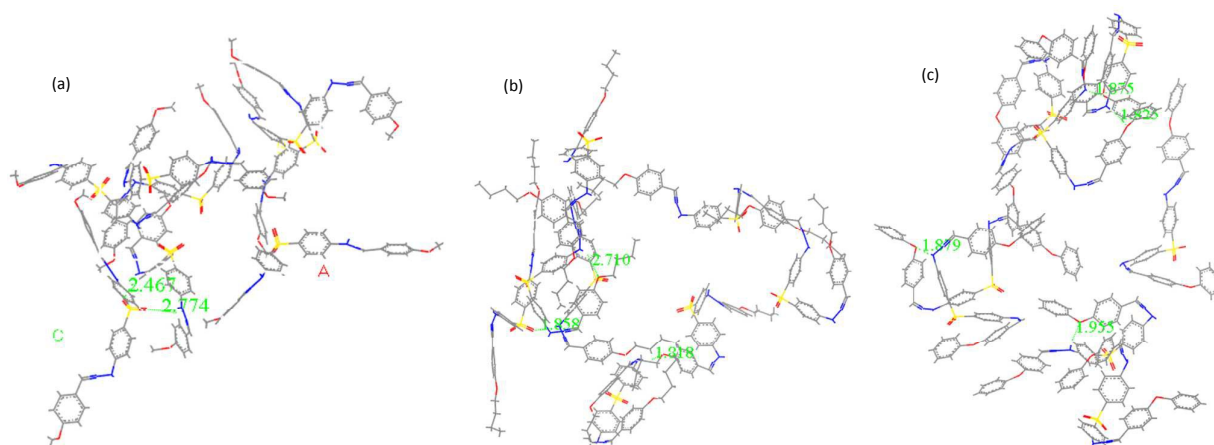

Fig.7 Packing mode of BAHDS-1(a), BAHDS-2(b) and BAHDS-4(c) computed by MD method
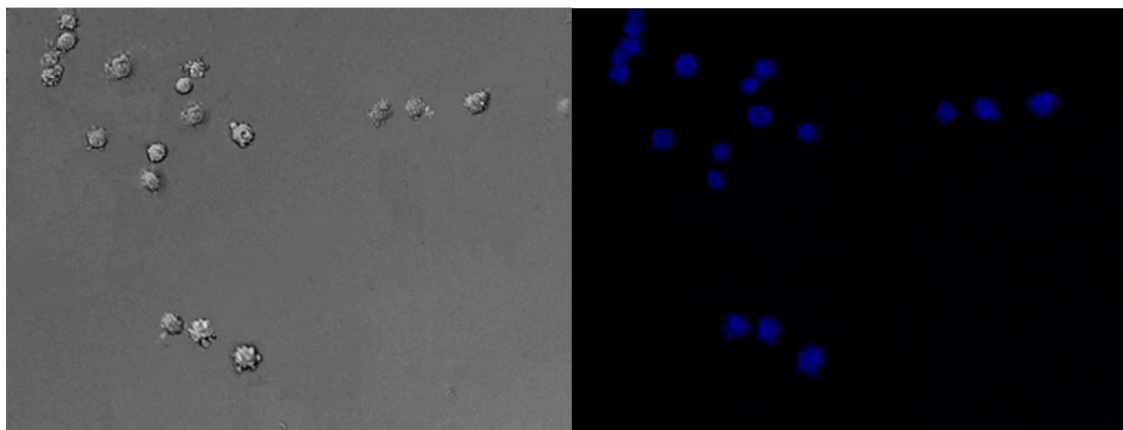
3.5 living cell imaging

Fig.8 Fluorescence images of A549 treated with 50 μg.mL^{-1} BAHDS-1 under visible light (left) and UV irradiation (right).

Living cell imaging of A549 was obtained at 450 nm (λ = 380 nm) by inverted fluorescence microscope. The cells displayed a bright blue fluorescence image. The fluorescence images were depicted in Fig.8. The fluorescence and bright-field images revealed a high cell membrane permeability of BAHDS-1.

To confirm the formation of aggregation inside the cells, small amount of BAHDS-1 was added to the cell culture fluid to simulate the cell environment, and dynamic light scattering (DLS) measurement was conducted. As it was shown in Fig.9, the average diameter of the particle was 391.5nm, which indicated the formation of aggregation inside the cells. BAHDS-1 could probably permeate the cell membrane in the solution state, and aggregate inside the cell. These results demonstrated that the BAHDS-1 was

cell membrane permeable and can also be used for the imaging of cells. [49-51]

As for intracellular imaging applications, the cytotoxicity of the probe should be taken into consideration. The MTT assay was performed to evaluate the toxicity of BAHDS-1 by A549 cells. 8-16-24 h incubation was taken at the same condition. The experimental data were expressed in Table 3. BAHDS-1 exhibited little cytotoxicity for cells, and at the concentration of 20 μM, the cell viability was still more than 85%. This result demonstrates that BAHDS-1 had a good biocompatibility.

Concentration of BAHDS-1 ($\times 10^{-5}$ mol·L^{-1})	Cell survival		
	8h	16h	24h
0	99%	98%	98%
0.5	98%	98%	96%
1	97%	95%	94%
1.5	95%	92%	90%
2	93%	89%	85%

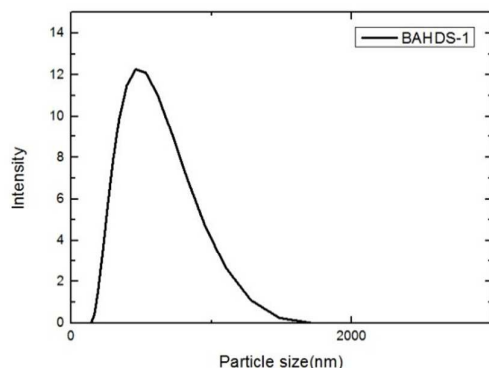**Table 3** Cell survival with 0, 0.5, 1, 1.5, 2 mol·L^{-1} BAHDS-1 after 8, 16, 24h.

Fig.9 DLS data of BAHDS-1 in the cell culture fluid.

Conclusions

BAHDS derivatives were designed and synthesized, and their structures were characterized by NMR, IR, and element analysis. The investigation of photo-physical properties displayed the strong AIE effect of BAHDS in THF/water mixture solvent. The maximum enhancement was 228.4 times of that in pure THF. Fluorescent microscope imagines showed blue fluorescence in THF/water mixture solvent, which attributed to the formation of the aggressive state. The mechanism of aggregation induced emission (AIE) was supported by molecular dynamic calculations. The results depicted that the packing mode and intermolecular hydrogen bond inhibited the intramolecular rotation and prevented π-π stacking, which caused AIE effect. Living cell imaging considered that BAHDS derivatives had good cell permeability and distinct blue fluorescence in A549 living cells. It was successfully applied to living cells staining, which demonstrated its value for practical applications in physiological systems.

Acknowledgements

Notes and references

1   C. C. Coleman, A. B. Epstein and R. J. Ebert, *J. Phys. Chem. Solids*, 1993, 11, 1497-1500.
2   M. Ananda, A. M. B. R. Sarker, D. C. Wheaton and Neckers, *Macromolecules*, 1997, 30, 2268-2273.
3   Y. M. Dong, D. Navarathne, A. Bolduc, N. McGregor andW. G. Skene, *J. Org. Chem.*, 2012, 77, 5429-5433.
4   H. J. Cho, K.Seo, C. J. Lee,H. Yun and J. Y. Chang, *J. Mater. Chem.*, 2003, 13, 986-990.
5   A. Igarashi, K. Arimitsu, T. Seki and K. Ichimura, *J. Mater. Chem.*, 2008, 18, 560-566.
6   B. D. Lourdes, N. David, Reinhoudt and C. C. Mercedes, *Chem. Soc. Rev.*, 2007, 36, 993-1017.
7   Y. C. Li, X.L. Li, X. Y. Cai, D. C. Chen, X. Liu, G. Z. Xie, Z. H. Wang, Y. C. Wu, C. C. Lo, A. Lien, J. B. Peng, Y. Cao and S. J. Su, *J. Mater. Chem. C*, 2015, 3, 6986-6996.
8   H. S. P. Rao and A. Desai, *RSC Adv.*, 2014, 4, 63642-63649.
9   G. J. Chang, L. Yang, S. Y. Liu, R. X. Lin and J. S. You, *Polym. Chem.*, 2015, 6, 697-702.
10 Y. Takagi, T. Kunishi, T. Katayama, Y. Ishibashi, H. Miyasaka, M. Morimoto and M.Irie, *Photochem.Photobiol. Sci.*, 2012, 11, 1661-1665.
11 J. L. Geng, K. I. Li, D. Ding, X. H. Zhang, W. Qin, J. Z. Liu,B. Z. Tang and B. Liu, *Small*, 2012, 8, 3655.
12 Y. N. Hong, J. W. Y. Lam and B. Z. Tang, *Chem. Commun.*, 2009, 4332–4353.
13 Y. N. Hong, J. W. Y. Lam and B. Z. Tang, *Chem. Soc. Rev.*, 2011, 40, 5361–5388.
14 C. W. Tang and S. A. Vanslyke, *Appl. Phys. Lett.*, 1987, 51, 913.
15 C. D. Geddes and J. R. Lakopwicz, *Advanced Concepts in Fluorescence Sensing*, Springer, Norwell, 2005.
16 H. Wang, E. Zhao, J. W.Y. Lam and B. Z. Tang, *Mater. Today.*, 2015, 18, 365-377.
17 X. L. Yang, G. J. Zhou and W. Y. Wong, *Chem. Soc. Rev.*, 2015, 44, 8484-8575.
18 X. L. Yang, X. B. Xu and G. J. Zhou, *J. Mater. Chem. C*, 2015, 3, 913-944.
19 Y. H. Chen and D. G. Ma, *J. Mater. Chem.*, 2012, 22, 18718-18734.
20 U. Mitschke and P.Bäuerle, *J. Mater. Chem.*, 2000, 10, 1471-1507.
21 L. Duan, L. D.Hou, T. W. Lee, J.Qiao, D. Q. Zhang, G. F. Dong, L. D. Wang and Y.Qiu, *J. Mater. Chem.*, 2010,20, 6392-6407.
22 B. Huang, Z. H. Yin, X. X. Ban, Z. M. Ma, W. Jiang, W. W. Tian, M. Yang, S. H. Ye, B. P. Lin and Y. M. Sun, *J. Lumin.*, 2016, 172, 7-13.
23 Y. L.Lv, Y. X. Hu, J. H. Zhao, G. W. Zhao, Y. Qi, X. Li, H. J. Chi, Y. Dong, G. Y. Xiao and Z. S. Su, *Opt. Mater.*, 2015, 49, 286-291.
24 G. W. Zhao, Y. X. Hu, H. J. Chi, Y. Dong, G. Y. Xiao, X. Li and D. Y. Zhang, *Opt. Mater.*, 2015, 47, 173-179.
25 B. Z. Tang, *Chem Mater*, 2003;15:1535-1546.
26 J. Luo, Z. Xie, J. W. Y. Lam, L. Cheng, H. Chen, C. Qiu,H. S. Kwok, X. Zhan, Y. Liu, D. Zhu and B. Z. Tang, *Chem. Commun.*, 2001, 1740.
27 B. Z. Tang, X. Zhan, G. Yu, P. P. S. Lee, Y. Liu and D. Zhu, *J. Mater. Chem.,* 2001, 11, 2974.
28 J. W. Chen, Z. L. Xie, J. W. Y. Lam, C. C. W. Law andB. Z. Tang, *Macromolecules,* 2003, 36, 1108—1117.
29 Z. J. Zhao, S. M. Chen, J. W. Y. Lam, P. Lu, Y. C. Zhong,K. S. Wong, H. S. Kwok andB. Z. Tang, *Chem. Comm.,* 2010, 46, 2221-2223.
30 H.Tong, Y. Hong andY. Dong, *J. Phys. Chem. B,* 2007, 118, 2000-2007.
31 B. K. An, S. K. Kwon andS. D. Jung, *J. Am. Chem. Soc.*, 2002, 124, 14410-14415.
32 H. Xi, C. X. Yuan, Y. X. Li, Y. Liu and X. T. Tao, *CrystEngComm*, 2012, 14, 2087.
33 C. X. Yuan, X. T. Tao, L. Wang, J. X. Yang, and M. H. Jiang, *J. Phys. Chem. C*, 2009, 113, 6809–6814
34 X. F. Mei, G. X. Wen, J. W. Wang, H. M. Yao, Y. Zhao, Z. H. Lin and Q. D. Ling, *J. Mater. Chem. C*, 2015, 3, 7267.

ARTICLE

35 S.A. Svarovsky, R.H. Simoyi, and S.V. Makarov, *J. Phys. Chem. B*, 2001, 105, 12634.

36 A.D. Becke, *J. Chem. Phys.* 1993, 98, 5648.

37 A.D. Becke, *J. Chem. Phys.* 1992, 96, 2155.

38 M. J. Frisch, G. W. Trucks, H. B. Schlegel, G. E. Scuseria, M. A. Robb, J. R. Cheeseman, G. Scalmani, V. Barone, B. Mennucci, G. A. Petersson, H. Nakatsuji, M. Caricato, X. Li, H. P. Hratchian, A. F. Izmaylov, J. Bloino, G. Zheng, J. L. Sonnenberg, M. Hada, M. Ehara, K. Toyota, R. Fukuda, J. Hasegawa, M. Ishida, T. Nakajima, Y. Honda, O. Kitao, H. Nakai, T. Vreven, J. A. Montgomery, Jr, J. E. Peralta, F. Ogliaro, M. Bearpark, J. J. Heyd, E. Brothers, K. N. Kudin, V. N. Staroverov, R. Kobayashi, J. Normand, K. Raghavachari, A. Rendell, J. C. Burant, S. S. Iyengar, J. Tomasi, M. Cossi, N. Rega, J. M. Millam, M. Klene, J. E. Knox, J. B. Cross, V. Bakken, C. Adamo, J. Jaramillo, R. Gomperts, R. E. Stratmann, O. Yazyev, A. J. Austin, R. Cammi, C. Pomelli, J. W. Ochterski, R. L. Martin, K. Morokuma, V. G. Zakrzewski, G. A. Voth, P. Salvador, J. J. Dannenberg, S. Dapprich, A. D. Daniels, O. Farkas, J. B. Foresman, J. V. Ortiz, J. Cioslowski and D. J. Fox, *Gaussian 09 Revision A.02,* Gaussian Inc., Wallingford CT, 2009.

39 J. Tomasi, and M. Persico, *Chem Rev*, 1994, 94, 2027.

40 M. P. Allen, and D. J. Tildesley, *Computer Simulation of Liquids*, Oxford University Press, New York, 1987.

41 S. Nosé, *J. Chem. Phys.*, 1984, 81, 511-519.

42 Z. Zhao, S. Chen, X. Shen, F. Mahtab, Y. Yu, P. Lu, J. W.Y. Lam, H. S. Kwok and B. Z. Tang, *Chem. Commun.*, 2010,46, 686.

43 R. Katoh, S. Katoh, A. Furube, K. Tokumaru and M. Kotani,*J. Phys. Chem. C*, 2009, 113, 2961.

44 Z. Zhao, S. Chen, J. W. Y. Lam, P. Lu, Y. Zhong, K. S. Wong,H. S. Kwok and B. Z. Tang, *Chem. Commun.*, 2010, 46, 2221.

45 M.Sarma, T. Chatterjee, S.Ghanta, and S. K. Das, *J. Org. Chem.* 2012, 77, 432−444.

46 X. Q. Zhang, M. Y. Liu, B. Yang, X. Y. Zhang and Y. Wei, *Colloid. Surface. B.*, 2013, 112, 81-86.

47 J. Mei, Y. Hong, J. W. Y. Lam, A. Qin, Y. Tang andB. Z. Tang, *Adv Mater*, 2014, 26, 5429−5479.

48 T. Y. Han, W. Wei, J. Yuan, Y. Duan, Y. P. Li, L. Y. Hu andY. P. Dong, *Talanta,* 2016:150:104-112.

49 Y. L. Xu, W. Yang, J. Shao, W. Q. Zhou, W. Zhu and J.Xie, *RSC Adv.*, 2014, 4, 15400.

50 W. Yang, Z. Q. Cheng, Y. L. Xu, J. Shao, W. Q. Zhou, J.Xie and M. Y. Li, *New J. Chem.*, 2015,39, 7488.

51 J. Cao, C. C. Zhao, X. Z. Wang, Y. F. Zhang and W. H. Zhu, *Chem. Commun.*, 2012, 48, 9897−9899.
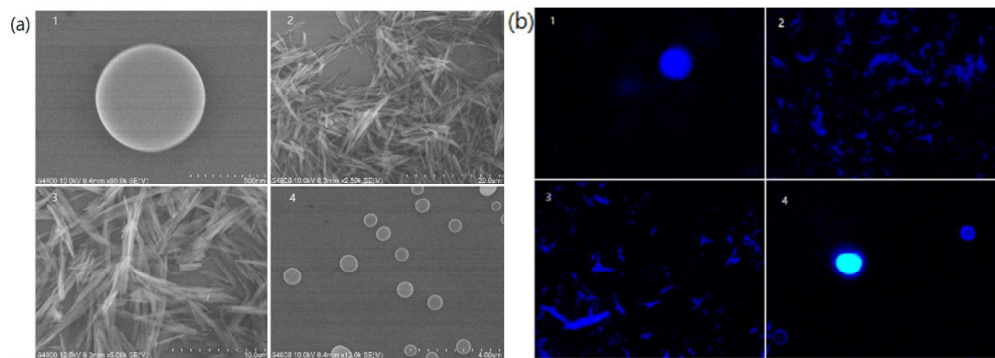
The SEM and fluorescence microscope image of BAHDS derivatives showed its nanoscale size and the strong fluorescence in solid state.